Journal of Materials Chemistry C

ROYAL SOCIETY OF CHEMISTRY

PAPER

View Article Online
View Journal | View Issue

Cite this: J. Mater. Chem. C, 2021, 9, 11292

$CaY_2Al_4SiO_{12}:Ce^{3+},Mn^{2+}$: a single component phosphor to produce high color rendering index WLEDs with a blue chip†

Qiuhong Zhang,[a] Junhao Li,*[a] Wei Jiang,[a] Litian Lin,[a] Jianhong Ding,[a] Mikhail G. Brik,[bcd] Maxim S. Molokeev,[efg] Haiyong Ni*[a] and Mingmei Wu*[h]

Received 16th April 2021,
Accepted 18th July 2021

DOI: 10.1039/d1tc01770e

rsc.li/materials-c

A high color rendering index white light emitting diode (WLED) is generally produced by combining yellow and red mixed phosphors on a blue chip. Herein we report a single component phosphor based on $CaY_2Al_4SiO_{12}$ (CYAS) to achieve warm white light emission with a high color rendering index (R_a), which can be up to 90.5. Ce^{3+}, Mn^{2+} singly doped and co-doped CYAS phosphors have been synthesized by solid state reactions, respectively, for comparative investigations. The Rietveld X-ray diffraction (XRD) refinements show that the CYAS host crystallizes in a cubic structure with the $Ia\bar{3}d$ space group. The valence states of Ce and Mn inside the CYAS host have been confirmed by XPS and EPR. Ce^{3+} occupies the Ca^{2+}/Y^{3+} site and generates a yellow emission band around 543 nm from its characteristic 5d–4f transition. Mn^{2+} occupies both the dodecahedron Ca^{2+}/Y^{3+} and octahedral Al^{3+} sites, emitting red and deep red lights at 616 nm and 750 nm, respectively. These two emission bands are attributed to the $^4T_1(^4G)-^6A_1(^6S)$ transitions of Mn^{2+}. Upon 460 nm light excitation, both the Ce^{3+} and Mn^{2+} characteristic emissions can be obtained, in which the emissions of Mn^{2+} result from the occurrence of energy transfer from Ce^{3+} in CYAS. All the results indicate that the prepared CYAS:-Ce^{3+},Mn^{2+} could be a promising single component phosphor for blue chip WLEDs.

1. Introduction

Recently, increasing attention has been paid to phosphor-converted WLEDs (pc-WLEDs) due to their excellent properties, such as high efficiency, energy conservation, long life time, and environment-friendly features.[1–3] The most popular way to obtain WLEDs is the combination of the yellow emitting phosphor $Y_3Al_5O_{12}:Ce^{3+}$ (YAG:Ce^{3+}) with a blue InGaN LED chip.[4,5] However, such white light lacks the red spectral component and thus the color rendering index is low (Ra $<$ 80) and the correlated color temperature is high (CCT $>$ 6000 K). It falls behind the increasing demand of high quality lighting.[6–9] To improve the color rendering index, one approach is to introduce red phosphor.[10,11] However, the difference in degradation between different components will lead to undesirable color aberration in application. What is worse, the mixed use of multiple phosphors causes a huge increase in production costs.

Due to the aforementioned reasons, considerable efforts have been devoted to enhancing red emissions in YAG:Ce^{3+} phosphor, for the purpose of achieving a higher color rendering index. In general, there are two main strategies to enhance the red emission of the YAG:Ce^{3+} system. One is to construct a solid solution to modify the crystal field strength to enhance the red emission fraction of YAG:Ce^{3+}.[12–17] The other is by co-doping of red light emitting activators in Ce^{3+} doped garnets, such as Cr^{3+}, Pr^{3+} and Sm^{3+}.[18–20] However, due to the narrow emission peaks of these ions, the red emission fraction cannot be enhanced effectively.

Mn^{2+} ions could exhibit a varying broad band emission from green to deep red depending on the host lattice. Mn^{2+} ions in a weak crystal field can emit green light, while Mn^{2+} ions in a strong crystal field would give rise to a red emission. Mn^{2+} ions can emit both orange red and deep red emissions in garnets, and thus utilizing Mn^{2+} to enhance the red emission of Ce^{3+} doped garnet phosphors based on the energy transfer from Ce^{3+}

[a] Guangdong Province Key Laboratory of Rare Earth Development and Application, Institute of Rare Metals, Guangdong Academy of Sciences, Guangzhou 510651, P. R. China. E-mail: 327481344@qq.com, nhygd@163.com
[b] College of Sciences & CQUPT-BUL Innovation Institute, Chongqing University of Posts and Telecommunications, Chongqing, 400065, P. R. China
[c] Institute of Physics, University of Tartu, W. Ostwald Str. 1, Tartu 50411, Estonia
[d] Faculty of Science and Technology, Jan Dlugosz University, Armii Krajowej 13/15, PL-42200, Częstochowa, Poland
[e] RAS, Fed. Res. Ctr KSC SB, Kirensky Inst. Phys., Lab Crystal Phys, Krasnoyarsk 660036, Russia
[f] Siberian Fed Univ., Krasnoyarsk 660041, Russia
[g] Far Eastern State Transport Univ., Dept. Phys., Khabarovsk 680021, Russia
[h] School of Marine Sciences, Sun Yat-Sen University, Zhuhai 510275, P. R. China. E-mail: ceswmm@mail.sysu.edu.cn

† Electronic supplementary information (ESI) available. See DOI: 10.1039/d1tc01770e

to Mn^{2+} has attracted great attention.[21–29] It has been reported that Ce^{3+}/Mn^{2+} co-doped $Y_3Al_5O_{12}$ phosphors can realize the optimization of the R_a value from 61.8 to 82.5 in WLEDs.[27] If $Y_3MgAl_3SiO_{12}$:Ce^{3+},Mn^{2+} phosphor is used on a blue chip, an increase of the R_a value to 85.4 can be achieved.[28] These all prove that the color rendering index can be improved by doping an appropriate amount of Mn^{2+} ions in a garnet host. However, the R_a is still not high enough for high-quality warm-white lighting. Mn^{2+} ions cannot supplement sufficient red fraction in traditional YAG garnet. Modifications on YAG garnet by co-substitution of Y–Al or Al–Al by Mg–Si pairs allows Mn^{2+} to emit efficient red light. However, such modifications is accompanied by an unexpected red shift of Ce^{3+} emission, making it difficult to further improve R_a in Ce^{3+}–Mn^{2+} co-doped systems. Therefore, it is necessary to explore a suitable host for solving the above problem. $CaY_2Al_4SiO_{12}$ (CYAS) garnet has been designed by modifying the known YAG garnet by co-substitution of Y–Al by Ca–Si pairs. CYAS can provide charge-matched sites for Mn^{2+}; simultaneously, the incorporation of Ca^{2+}–Si^{4+} into Y^{3+}–Al^{3+} pairs of YAG enables shift of the Ce^{3+} emission to shorter wavelengths.[30] Therefore, a higher R_a can be expected by co-doping Ce^{3+} and Mn^{2+} in the CYAS garnet. Furthermore, the origin of the deep red emission at around 750 nm in garnets is still unclear. A few research groups point out that the 750 nm emission may be related to the emission of Mn^{3+},[31,32] while some believe that the deep red emission comes from Mn^{2+} in the dodecahedron, and some believe that it could be ascribed to Mn^{2+} in the octahedron or even in the tetrahedron.[21,26–29] It is significant to confirm the site occupation of Mn^{2+} in the garnet structure, which determines the spectral properties and eventually affects the suitability of phosphors in LED applications.

In this work, a novel $CaY_2Al_4SiO_{12}$:Ce^{3+},Mn^{2+} (CYAS:Ce^{3+},Mn^{2+}) phosphor has been prepared. The crystal structure of the CYAS host, valence state and site occupancy of the dopants, mechanism of energy transfer, and behavior of thermal quenching have been investigated in detail. Results indicate that, in this CYAS garnet, cerium and manganese are present in the valence states of +3 and +2, respectively. Ce^{3+} occupies only the Ca^{2+}/Y^{3+} site, while Mn^{2+} occupies both the Ca^{2+}/Y^{3+} dodecahedron and Al^{3+} octahedron sites. Ce^{3+} in CYAS generates a yellow emission band at 543 nm, while Mn^{2+} emits red and deep red lights at 616 nm and 750 nm, respectively. Upon 460 nm light excitation, the Ce^{3+}–Mn^{2+} energy transfer enables the as-prepared phosphors to produce a wide range of emissions covering nearly the whole visible spectral region. Additionally, the CYAS:Ce^{3+},Mn^{2+} phosphor exhibits satisfactory thermal stability and the quenching temperature $T_{0.5}$ can be above 473 K. Finally, the white LED with a high color rendering index (R_a = 90.5) and a suitable correlated color temperature (CCT = 5460 K) can be fabricated with the CYAS:0.02Ce^{3+},0.25Mn^{2+} phosphor and a blue LED chip.

2. Experimental section

2.1 Syntheses

Phosphors with the compositions of $Ca_{1-x}Y_{1.98}Al_4SiO_{12}$:0.02Ce,$x$Mn ($x$ = 0.00, 0.05, 0.10, 0.15, 0.20, 0.25, and 0.30) and $Ca_{0.9}Y_2Al_4SiO_{12}$:0.1Mn were synthesized by solid state reaction technology. $CaCO_3$ (A.R.), SiO_2 (A.R.), $MnCO_3$ (A.R.), Y_2O_3 (99.995%), Al_2O_3 (99.99%) and CeO_2 (99.995%) were used as the starting materials and NH_4Cl (A.R.) was used as the flux, respectively. Stoichiometric amounts of starting materials and 0.3 wt% of NH_4Cl flux were thoroughly mixed by grinding in an agate mortar. The mixture was pre-fired at 873 K for 1.0 hour and finally sintered at 1673 K for 4.0 hours under a reductive atmosphere (75% N_2 + 25% H_2), followed by intermediate grinding.

2.2 Characterization

The powder X-ray diffraction (XRD) test was carried out by using a Bruker D8 Advance diffractometer with Cu Kα radiation (λ = 1.54056 Å) at 40 kV and 40 mA. The refinement of crystal structure was performed using TOPAS-Academic V4.1 (Coelho, A. TOPAS-Academic, Version 4.1; Coelho Software: Brisbane, Australia, 2007). The X-ray photoelectron spectroscopy (XPS) measurements were performed in a Thermo Scientific NEXSA spectrometer (Thermo Fisher, USA) with a monochromatic Al Kα X-ray source ($h\nu$ = 1486.6 eV, 15 kV and 15 mA). The electron spin resonance (EPR) spectra of Mn ions were obtained with a Bruker A300 X-band (ν = 9.29 GHz) spectrometer at 100 K. The photoluminescence (PL) and photoluminescence excitation (PLE) spectra at room temperature were recorded using a Hitachi F7000 fluorescence spectrophotometer, equipped with a 450 W xenon lamp as the excitation source. The temperature dependent PL spectra were measured using a Hitachi F7000 spectrofluorometer equipped with a 450 W Xenon lamp. The decay curves were obtained by using an FLS1000-Combined Fluorescence Lifetime and Steady State Spectrometer (Edinburgh Instruments) equipped with Xe/μs lamps. The quantum efficiency of the synthesized samples was measured by using a QY-2000 equipped with a 460 nm blue LED lamp (Orient Koji, China). $BaSO_4$ was used as a standard reference in the measurements. Electroluminescence (EL) analysis of the fabricated white LED was conducted using the LED300E programmable test powder for LEDs (EVERFINE, China).

3. Results and discussion

3.1 Crystal structure characteristics

Rietveld refinement was implemented with the crystallographic data of $Y_3Al_5O_{12}$ (ICSD #23848) as a starting model to study the structure of the prepared CYAS phosphor. The observed and calculated results and their differences are depicted in Fig. 1a. The observed pattern matches well with the calculated one. The obtained fitting parameters are R_{wp} = 11.57%, R_p = 8.04% and R_{exp} = 3.70%. The prepared CYAS forms a single phase and crystallizes in a cubic structure with the $Ia\bar{3}d$ space group. The lattice parameters are $a = b = c$ = 11.9770(6) Å, $\alpha = \beta = \gamma = 90^\circ$, V = 1718.07(25) Å^3 and Z = 8 (Table 1). The CYAS retains the typical garnet structure as shown in Fig. 1b. Due to the similar ionic radii for Ca^{2+} ions (R_{Ca} = 1.12 Å for CN = 8) and Y^{3+} ions (R_Y = 1.02 Å for CN = 8), Ca^{2+} substitutes for Y^{3+} in the chemical formula of $Y_3Al_5O_{12}$. Ca and Y atoms are located at the 24c site

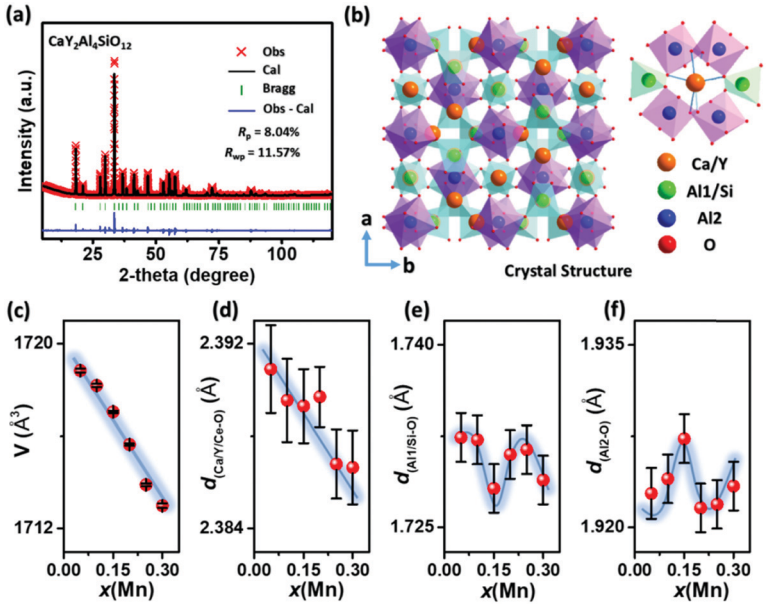

Fig. 1 (a) Rietveld refinement of powder X-ray patterns, (b) crystal structure of $CaY_2Al_4SiO_{12}$, and (c) cell volume V and (d) bond lengths of $d_{(Ca,Y-O)}$, (e) $d_{(Al1,Si-O)}$, and (f) of $d_{(Al2-O)}$ depending on Mn concentration (x).

(coordinate with eight oxygen ions to form a $(Ca,Y)O_8$ dodecahedron), while Al atoms are located at two different Wyckoff positions, *i.e.*, Al1 shares the 24d site with Si to form a $(Al,Si)O_4$ tetrahedron (because of the similar ionic radii (R_{Si} = 0.40 Å, R_{Al} = 0.53 Å for CN = 4)) and Al2 at the 16a site to form an AlO_6 octahedron.

To determine the influence of Ce, Mn on the CYAS crystal structure, the phase purity of the prepared phosphors CYAS:0.02Ce,xMn (x = 0.00, 0.05, 0.10, 0.15, 0.20, 0.25, and 0.30) has been identified by powder XRD (Fig. S1, ESI†). It is obvious that their diffraction peaks match well with those of the cubic CYAS, indicating that the addition of Ce and Mn ions did not change the main cubic crystal structure. The cell volume V, $d_{(Ca/Y/Ce-O)}$, $d_{(Al1/Si-O)}$ and $d_{(Al2-O)}$ depending on Mn concentration (x) are shown in Fig. 1c–f, respectively. The cell volume V and the average bond length of $d_{(Ca/Y/Ce-O)}$ noticeably decrease with increasing Mn concentration as shown in Fig. 1c and d, respectively. However, the variation of the average bond length of neither $d_{(Al1/Si-O)}$ nor $d_{(Al2-O)}$ is regular (Fig. 1e and f), confirming that the Mn can preferentially occupy the Ca^{2+}/Y^{3+} sites in CYAS. The valence states of Ce and Mn have been further investigated by XPS and EPR, confirming that they are Ce^{3+} and Mn^{2+}, respectively (Fig. S2, ESI†).

3.2 Luminescence properties of Ce^{3+}, Mn^{2+} singly- and co-doped CYAS phosphors

The PL and PLE spectra of CYAS:Ce^{3+} are shown in Fig. 2a. Monitoring at 543 nm, two broad bands centered at 345 nm and 460 nm are observed, which originate from the 4f–5d transitions of Ce^{3+} ions. Under excitation at 460 nm, CYAS:0.02Ce^{3+} gives a yellow emission band peaking at around 543 nm, which originated from the 5d–4f transitions of Ce^{3+}. Fig. 2b shows the PL and PLE spectra of CYAS:Mn^{2+}. The PLE spectrum of CYAS:Mn^{2+} (monitored at 616 nm) shows typical d–d transitions of Mn^{2+}. The PL spectrum of CYAS:Mn^{2+} under 410 nm excitation exhibits two weak broad emission bands at around 616 nm Mn^{2+}(I) and 750 nm Mn^{2+}(II), respectively. The two bands correspond to the spin forbidden $^4T_1(^4G)$–$^6A_1(^6S)$ transitions of Mn^{2+}. The appearance of two bands indicates that Mn^{2+} may locate in two different crystallographic sites in CYAS, possibly related to the Al^{3+} octahedral site and the Ca^{2+}/Y^{3+} dodecahedral site, respectively, considering that the ionic radius of Mn^{2+} (R_{Mn} = 0.67 Å for CN = 6 and R_{Mn} = 0.93 Å for CN = 8) is similar to that of Al^{3+} (R_{Al} = 0.53 Å, CN = 6) and (R_Y = 1.02 Å, CN = 8 and R_{Ca} = 1.12 Å). The Mn^{2+} emission position is strongly dependent on the crystal-field environment of the host lattice. When the crystal-field around Mn^{2+} becomes stronger, the emission band will shift towards a lower energy because of larger splitting of the $^4T_1(^4G)$ orbital triplet.

The crystal field theory was used to analyze the crystal field strength at both sites occupied by the Mn^{2+} ions. Comparison of the crystal field strengths for different sites will unambiguously identify the site with a stronger crystal field and larger

Table 1 Rietveld refined crystallographic data of CYAS[a]

Atom	Wyck.	x/a	y/b	z/c	Occ.	B_{iso}
Al1	16a	0	0	0	1	2.1768
Al2	24d	0.3750	0	0.2500	0.66667	2.1768
Si1	24d	0.3750	0	0.2500	0.33333	2.1768
Y1	24c	0.1250	0	0.2500	0.66667	1.13147
Ca1	24c	0.1250	0	0.2500	0.33333	1.13147
O1	96h	−0.02963	0.04927	0.15168	1	2.47511

[a] Crystal structure: cubic; space group: $Ia\bar{3}d$; $a = b = c$ = 11.9770 (6) Å, $\alpha = \beta = \gamma = 90°$, V = 1718.07 (25) Å^3, and Z = 8, R_{wp} = 11.57%, R_p = 8.04% and R_{exp} = 3.70%.

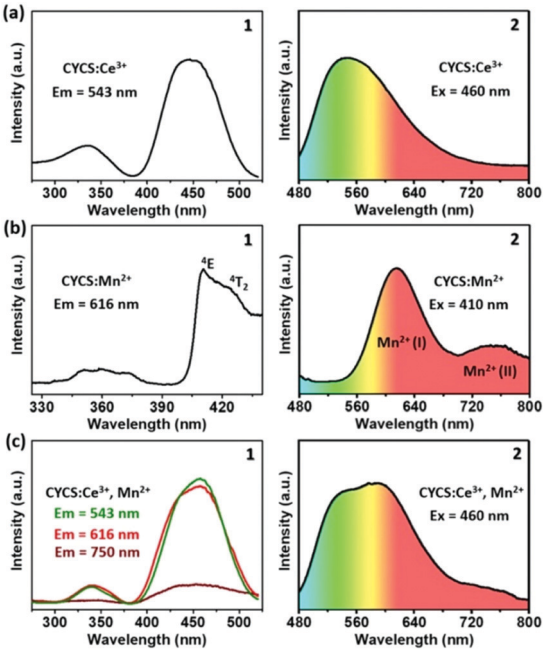

Fig. 2 PL and PLE spectra of (a) CYAS:Ce^{3+}, (b) CYAS:Mn^{2+}, and (c) CYAS:Ce^{3+},Mn^{2+}.

crystal field splittings. An explicit expression for the calculations of the crystal field strengths is as follows:[33]

$$N_v = \left[\sum_{k,q} \frac{\left(B_q^k\right)^2}{2k+1}\right]^{1/2} \quad (1)$$

where B_q^k (for the d ions $k = 2, 4, -k \le q \le k$) are the crystal field parameters. Using the structural data determined in the present work for the title host and explicit expressions for the point charge contributions to the crystal field parameters (as described in ref. 34) and converting them to Weybourne normalization, the following N_v values were obtained for different Mn^{2+} sites in $CaY_2Al_4SiO_{12}$: N_v(Al) = 8681 cm^{-1} and N_v(Ca) = 2185 cm^{-1}. Therefore, a stronger crystal field at the Al site leads to a greater crystal field splitting of the $^4T_1(^4G)$ orbital triplet and, as a result, red shift of the Mn^{2+} emission.

Hence, the 616 nm Mn^{2+}(I) emission can be assigned to Mn^{2+} in the Ca^{2+}/Y^{3+} dodecahedral site with a weak crystal-field, while the 750 nm Mn^{2+}(II) emission is assigned to Mn^{2+} in the Al^{3+} octahedral site with a strong crystal-field.

The PLE and PL spectra of CYAS:Ce^{3+},Mn^{2+} are shown in Fig. 2c. The emission spectrum under 460 nm excitation exhibits three emission bands centered at 543 nm (green), 616 nm (red) and 750 nm (deep red). The decay curves of the green emission band, red emission band and deep red emission band have been obtained (Fig. S3, ESI†). The average decay time (τ) can be defined using the equation: $\tau = \int I(t)t\,dt / \int I(t)\,dt$. The average decay times for the green, red and deep red emission bands are 72.10 ns, 7.05 ms and 17.29 ms, respectively. Because the d–d transition of Mn^{2+} is a spin–forbidden transition, the decay time of Mn^{2+} is on a millisecond scale. Therefore, these three emission bands are originated from the 5d–4f transitions of Ce^{3+} ions and $^4T_1(^4G)$–$^6A_1(^6S)$ transitions of Mn^{2+} ions, respectively. The decay curves of Mn^{2+} do not coincide, which further confirms that Mn^{2+} ions occupy two different sites in the CYAS host. The profiles of the excitation spectra under 616 nm and 750 nm emissions of

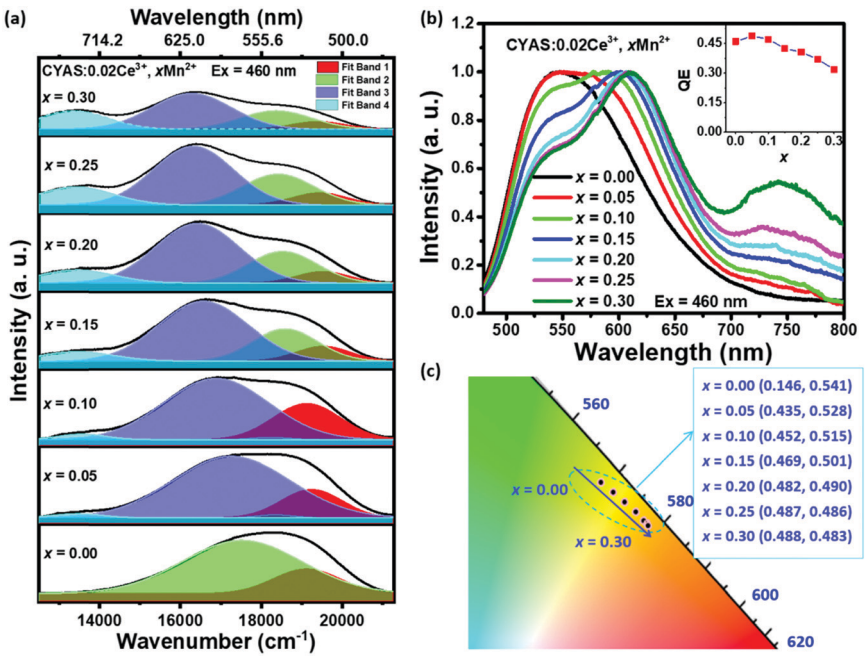

Fig. 3 (a) PL spectra and Gaussian curve fittings, (b) normalized PL spectra with the inset showing the variation of the quantum efficiency based on Mn^{2+} concentration x, and (c) CIE coordinates of CYAS:0.02Ce^{3+},xMn^{2+} (x = 0.00–0.30) phosphors (λ_{ex} = 460 nm).

Mn^{2+} are similar to that under 543 nm emission of Ce^{3+}, which gives a proof for the energy transfer from Ce^{3+} to Mn^{2+} in the CYAS host.

3.3 The energy transfer from Ce^{3+} to Mn^{2+} in the CYAS host

In order to investigate the energy transfer process involved in the CYAS:Ce^{3+},Mn^{2+} phosphor, the PL spectra and Gaussian curve fittings of CYAS:0.02Ce^{3+},xMn^{2+} phosphors (x = 0.00, 0.05, 0.10, 0.15, 0.20, 0.25, and 0.30) under 460 nm excitation were studied and are shown in Fig. 3a. The results indicate that the emission spectrum consists of two broad bands due to the 5d–4f transitions of Ce^{3+} ions when x = 0.00 (Fig. 3a, bottom). After the introduction of Mn^{2+} ions, the emission spectra can be fitted to four broad emission bands. Band 1 and band 2 are due to 5d–$^2F_{5/2}$ and 5d–$^2F_{7/2}$ transitions of Ce^{3+} ions, respectively. Band 3 (Mn^{2+}(I)) and band 4 (Mn^{2+}(II)) are due to $^4T_1(^4G)$–$^6A_1(^6S)$ transitions of Mn^{2+} ions. When $x \leq 0.10$, band 2 almost coincides with band 3, and band 4 is not obvious. Four emission bands can be obviously observed when $x > 0.10$.

Fig. 3b shows the normalized emission spectra of CYAS:0.02-Ce^{3+},xMn^{2+} (x = 0.00, 0.05, 0.10, 0.15, 0.20, 0.25, and 0.30) phosphors. The results indicate that the Ce^{3+} emission intensity decreases relative to the intensity of Mn^{2+}(I) emission, while the Mn^{2+}(II) emission intensity increases relative to the intensity of Mn^{2+}(I) emission with the increase of Mn^{2+} concentration. The normalized PLE spectra of CYAS:0.02Ce^{3+},xMn^{2+} (x = 0.00, 0.05, 0.10, 0.15, 0.20, 0.25 and 0.30) monitored at 543 nm were measured (for details see Fig. S4, ESI†). The absorption bands show a gradual red shift with the introduction of Mn^{2+}, which are attributed to the replacement of the bigger Ca^{2+}/Y^{3+} ions by Mn^{2+} ions. The quantum efficiency (QE) variation based on the Mn^{2+} concentration x is shown in the inset of Fig. 3b, indicating that the optimum QE of the Ce^{3+}, Mn^{2+} co-doped CYAS phosphor is about 48.77% at x = 0.05. The QE is about 36.94% for CYAS:0.02Ce^{3+},0.25Mn^{2+} phosphor. The CIE chromaticity coordinates of CYAS:0.02Ce^{3+},xMn^{2+} phosphors (x = 0.00, 0.05, 0.10, 0.15, 0.20, 0.25, and 0.30) phosphors are shown in Fig. 3c. The CIE coordinates of the phosphors vary from (0.146, 0.541) to (0.488, 0.483) with x values changing from 0.00 to 0.30, confirming that the content of red color increases with the increase of x value.

In order to further confirm the energy transfer between Ce^{3+} and Mn^{2+}, the decay curves of CYAS:0.02Ce^{3+},xMn^{2+} phosphors (x = 0.00, 0.05, 0.10, 0.15, 0.20, 0.25, and 0.30) were measured (Fig. S5, ESI†). The decay curve of the single Ce^{3+} doped sample is fitted well with a single-exponential decay mode. The decay curves of Ce^{3+} depart from the single-exponential decay mode for Mn^{2+} co-doped samples due to the energy transfer. The decay times of Ce^{3+} in CYAS:0.02Ce^{3+},xMn^{2+} phosphors decrease with the increase of Mn^{2+} content (Table S1, ESI†), confirming the possibility of energy transfer from Ce^{3+} to Mn^{2+} ions in the CYAS host. Further studies reveal that the energy transfer efficiency and rate of Ce^{3+}–Mn^{2+} increase with the increase of Mn^{2+} concentration when $x \leq 0.3$ and the dipole–dipole interaction dominates during the energy transfer from Ce^{3+} to Mn^{2+} ions in CYAS (for details see Fig. S6 and S7, ESI†). In addition, the schematic diagram of the energy transfer between Ce^{3+} and Mn^{2+} in CYAS is provided in Fig. S8, ESI.†

3.4 Application performance of phosphors in LEDs

In practical applications, thermal quenching behavior is a key factor affecting the luminescence performance. Therefore, it is very important to evaluate the thermal stability of CYAS:-Ce^{3+},Mn^{2+} phosphors. The temperature-dependent emission spectra of CYAS:0.02Ce^{3+},xMn^{2+} phosphors (x = 0.00, 0.10, and 0.25) were collected from 298 to 473 K (λ_{ex} = 460 nm). The temperature dependent emission spectra and normalized integrated emission intensities of CYAS:0.02Ce^{3+},xMn^{2+}

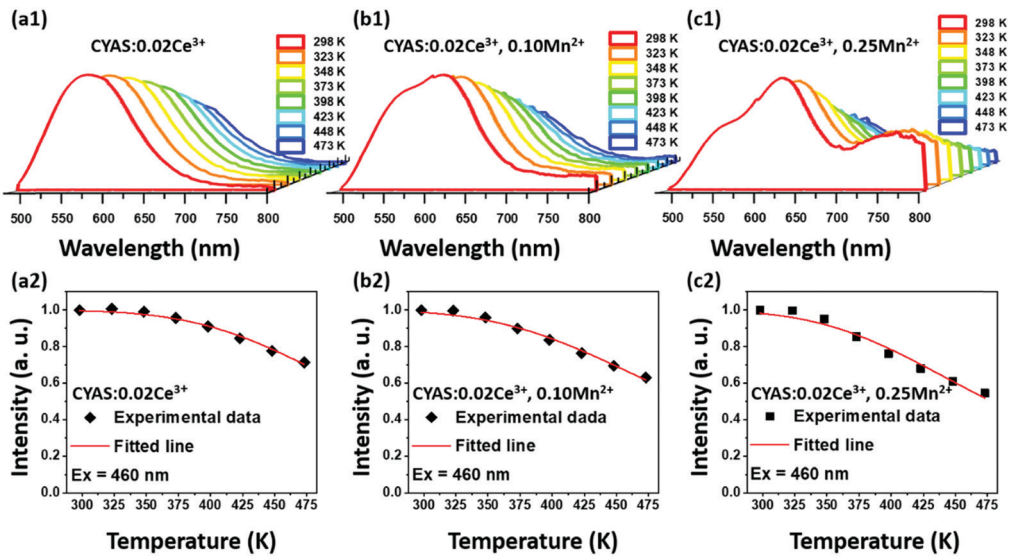

Fig. 4 (a1–c1) Temperature dependent emission spectra and (a2–c2) normalized integrated emission intensities of (a1 and a2) CYAS:0.02Ce^{3+} phosphor, (b1 and b2) CYAS:0.02Ce^{3+},0.10Mn^{2+} phosphor and (c1 and c2) CYAS:0.02Ce^{3+},0.25Mn^{2+} phosphor (λ_{ex} = 460 nm).

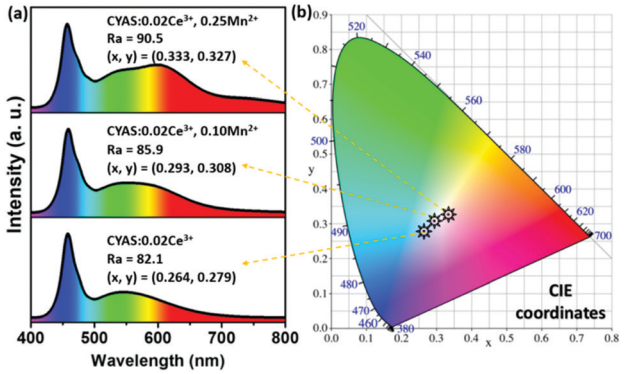

Fig. 5 (a) Electroluminescence spectra and (b) CIE coordinates of WLEDs fabricated by combining CYAS:0.02Ce^{3+},xMn^{2+} (x = 0.00, 0.10, and 0.25) phosphors and blue LED chips.

phosphors (x = 0.00, 0.10, and 0.25) under 460 nm light excitation are plotted in Fig. 4. The emission intensities decrease with the testing temperature as shown in Fig. 4(a1–c1). The integrated intensities of all the prepared phosphors at 373 K can remain above 85% of those at room temperature as shown in Fig. 4(a2–c2). The quenching temperature $T_{0.5}$, for which the intensity is half of the maximum intensity, have all been evaluated to be above 473 K for CYAS:0.02Ce^{3+},xMn^{2+} phosphors (x = 0.00, 0.10, and 0.25). The activation energy (ΔE) which is an important value to estimate the thermal stability of a phosphor has been calculated using the equation: $I_T = I_0/[1 + A\exp(-\Delta E/kT)]$.[35] They are determined to be 0.321 eV, 0.268 eV and 0.270 eV for x = 0.00, 0.10, and 0.25 in CYAS:0.02Ce^{3+},xMn^{2+} phosphors, respectively.

In order to investigate the potential application of CYAS:-Ce^{3+},Mn^{2+} phosphors in white LEDs, phosphor-converted LEDs (pc-LEDs) have been fabricated by combining blue LED chips with CYAS:0.02Ce^{3+},xMn^{2+} phosphors (x = 0.00, 0.10, and 0.25). The electroluminescence spectra and the CIE coordinates of the obtained white LEDs driven under a 100 mA forward bias current are shown in Fig. 5. The CIE chromaticity coordinates (x, y) are (0.264, 0.279), (0.293, 0.308) and (0.333, 0.327), and the correlated color temperatures (CCTs) are 13 092 K, 8089 K and 5460 K, respectively. The color rendering index can be up to 81.1, 85.9, and 90.5. The value of 90.5 is significantly higher than those reported in the literature (Table 2). The results indicate that the co-doping of Mn^{2+} in CYAS:0.02Ce^{3+} can obviously improve the color rendering index of the warm white LED with the chromaticity coordinates (0.333, 0.327).

Table 2 Comparison of CCT and CRI (R_a) of the WLEDs based on blue chips combined with different single component phosphors doped with Ce^{3+} and/or Mn^{2+}

Phosphors	CCT(K)	R_a	Ref.
CYAS:0.02Ce^{3+},0.25Mn^{2+}	5460	90.5	This work
YAG:0.02Ce^{3+}	7756	75	4
$Y_3Al_{4.8}Si_{0.2}O_{12}$:0.1$Ce^{3+}$,0.2$Mn^{2+}$	4162	82.7	24
$Lu_{1.2}Y_{1.8}Al_{4.8}Si_{0.2}O_{12}$:0.1$Ce^{3+}$,0.2$Mn^{2+}$	4387	84.8	24
$Y_{2.994}Ce_{0.006}Al_{4.68}Mn_{0.16}Si_{0.16}O_{12}$	3870	82.5	26
YMAS:0.08Ce^{3+},0.3Mn^{2+}	4502	85.4	27

The CYAS:Ce^{3+},Mn^{2+} phosphor is expected to be a potential single phase candidate with a high R_a for blue chip WLEDs.

4. Conclusions

A series of CYAS:0.02Ce^{3+},xMn^{2+} (x = 0.00, 0.05, 0.10, 0.15, 0.20, 0.25, and 0.30) phosphors were synthesized by solid state reactions. The Rietveld structure refinement results reveal that CYAS crystallizes as a cubic structure with a space group of $Ia\bar{3}d$. The Ca and Y atoms are located at the identical 24c site, while part of the Al atoms with octahedral coordination are located at the 16a site, and the other Al atoms with tetrahedral coordination share the identical 24d site with Si atoms in the CYAS host. The structural analysis and the luminescence properties confirm that the Ce^{3+} ions occupy the Ca^{2+}/Y^{3+} site, whereas the Mn^{2+} ions tend to occupy both the dodecahedron Ca^{2+}/Y^{3+} sites to generate a red emission band (616 nm) and octahedral Al^{3+} sites to generate a deep red emission band (750 nm) simultaneously. The energy transfer from Ce^{3+} to Mn^{2+} takes place in CYAS:Ce^{3+},Mn^{2+} phosphors *via* a dipole–dipole interaction and a much more efficient energy-transfer process occurs in the higher Mn^{2+} doped CYAS samples when $x \leq 0.3$. The quenching temperature of the prepared CYAS:0.02-Ce^{3+},xMn^{2+} (x = 0.00, 0.10, and 0.25) is above 473 K. White LEDs can be obtained by combining CYAS:Ce^{3+},Mn^{2+} phosphors with blue LED chips, and the Mn^{2+} co-doping can obviously improve the color rendering index of the white LED up to over 90.0. Therefore, CYAS:Ce^{3+},Mn^{2+} phosphor is a potential single component candidate for blue-chip based warm white LEDs.

Conflicts of interest

There are no conflicts to declare.

Acknowledgements

This work has been financially supported by the National Nature Science Foundation of China (51902063, 51902354, U1801253), the Science and Technology Project of Guangdong Province (2018A050506061), the Science and Technology Project of Guangzhou City (202007020005, 202007020008) and GDAS' Project of Science and Technology Development (2020GDASYL-20200 302010, 2018GDASCX-0110). M. G. Brik also thanks the support from the Chongqing Recruitment Program for 100 Overseas Innovative Talents (Grant No. 2015013), the Program for the Foreign Experts (Grant No. W2017011) and Wenfeng High-End Talents Project (Grant No. W2016-01) offered by Chongqing University of Posts and Telecommunications (CQUPT), Estonian Research Council grant PUT PRG111, European Regional Development Fund (TK141) and NCN project 2018/31/B/ST4/00924.

References

1 T. Taguchi, Y. J. Uchida, T. Setomoto and K. Kobashi, *Proc. SPIE*, 2001, **4278**, 7–12.

2 J. W. Qiao, L. X. Ning, M. S. Molokeev, Y. C. Chuang, Q. Y. Zhang, K. R. Poppelmeier and Z. G. Xia, *Angew. Chem., Int. Ed.*, 2018, **58**, 2–8.
3 J. H. Li, Q. Y. Liang, Y. F. Cao, J. Yan, J. B. Zhou, Y. Q. Xu, L. Dolgov, Y. Y. Meng, J. X. Shi and M. M. Wu, *ACS Appl. Mater. Interfaces*, 2018, **10**, 41479–41486.
4 H. S. Jang, Y. H. Won and D. Y. Jeon, *Appl. Phys. B: Lasers Opt.*, 2009, **95**, 715–720.
5 V. Bachmann, C. Ronda and A. Meijerink, *Chem. Mater.*, 2009, **21**, 2077–2084.
6 A. J. Huang, Z. G. Yang, C. Y. Yu, Z. Z. Chai, J. B. Qiu and Z. G. Song, *J. Phys. Chem. C*, 2017, **121**, 5267–5276.
7 P. Pust, P. J. Schmidt and W. Schnick, *Nat. Mater.*, 2015, **14**, 454–458.
8 Z. G. Xia and A. Meijerink, *Chem. Soc. Rev.*, 2017, **46**, 275–299.
9 J. Meyer and F. Tappe, *Adv. Opt. Mater.*, 2015, **3**, 424–430.
10 R. J. Xie, N. Hirosaki, N. Kimura, K. Sakuma and M. Mitomo, *Appl. Phys. Lett.*, 2007, **90**, 191101.
11 R. J. Xie, N. Hirosaki and M. Mitomo, *J. Electroceram.*, 2008, **21**, 370–373.
12 A. A. Setlur, W. J. Heward, Y. Gao, A. M. Srivastava, R. GopiChandran and M. V. Shankar, *Chem. Mater.*, 2006, **18**, 3314–3322.
13 M. M. Shang, J. Fan, H. Z. Lian, Y. Zhang, D. L. Geng and J. Lin, *Inorg. Chem.*, 2014, **53**, 7748–7755.
14 C. He, H. P. Ji, Z. H. Huang, T. S. Wang, X. G. Zhang, Y. G. Liu, M. H. Fang, X. W. Wu, J. Q. Zhang and X. Min, *J. Phys. Chem. C*, 2018, **122**, 15659–15665.
15 L. P. Jiang, X. Y. Zhang, H. Tang, S. Q. Zhu, Q. X. Li, W. M. Zhang, X. Y. Mi, L. P. Lu and X. L. Liu, *Mater. Res. Bull.*, 2018, **98**, 180–186.
16 X. Q. Zhou, J. W. Qiao and Z. G. Xia, *Chem. Mater.*, 2021, **33**, 1083–1098.
17 M. Zhao, Q. Y. Zhang and Z. G. Xia, *Acc. Mater. Res.*, 2020, **1**, 137–145.
18 H. S. Jang, W. B. Im, D. C. Lee, D. Y. Jeon and S. S. Kim, *J. Lumin.*, 2007, **126**, 371–377.
19 L. Wang, X. Zhang, Z. D. Hao, Y. S. Luo, X. J. Wang and J. H. Zhang, *Opt. Express*, 2010, **18**, 25177–25182.
20 H. Yang and Y. S. Kim, *J. Lumin.*, 2008, **128**, 1570–1576.
21 Y. R. Shi, Y. H. Wang, Y. Wen, Z. Y. Zhao, B. Liu and Z. G. Yang, *Opt. Express*, 2012, **20**, 21656–21664.
22 D. Pasiński, E. Zych and J. Sokolnicki, *J. Lumin.*, 2016, **169**, 862–867.
23 Y. C. Jia, Y. J. Huang, N. Guo, H. Qiao, Y. H. Zheng, W. Z. Lv, Q. Zhao and H. Q. You, *RSC Adv.*, 2012, **2**, 2678–2681.
24 Z. F. Pan, J. C. Chen, H. Q. Wu and W. Q. Li, *Opt. Mater.*, 2017, **72**, 257–264.
25 Y. L. Ma, L. Zhang, T. Y. Zhou, B. H. Sun, Y. Wang, J. Kang, P. Gao, J. Huang, F. A. Selim, C. P. Wong, M. Li and H. Chen, *J. Mater. Chem. C*, 2020, **8**, 4329–4337.
26 M. S. Cai, S. Q. Fang, T. Han, D. T. Valiev, T. C. Lang, Y. Zhong, C. L. Wang, A. N. Yakovlev and E. Polisadova, *J. Mater. Chem. C*, 2020, **8**, 14507–14514.
27 G. Ao, Y. R. Tang, X. Z. Yi, Y. N. Tian, J. Chen, D. M. Hao, Y. D. Lin and S. M. Zhou, *J. Alloys Compd.*, 2019, **798**, 695–699.
28 E. Tong, K. X. Song, Z. H. Deng, S. H. Shen, H. F. Gao, W. T. Su and H. P. Wang, *J. Lumin.*, 2020, **217**, 116787.
29 W. Xu, D. Q. Chen, Y. Zhou, J. S. Zhong and S. C. Li, *J. Mater. Chem. C*, 2017, **5**, 738–746.
30 J. J. Jia, Y. H. Qiang, J. F. Xu, M. Z. Liang, W. Wang, F. L. Yang, J. Cui, Q. Dong and X. Y. Ye, *J. Am. Ceram. Soc.*, 2020, 1–9.
31 S. Kück, S. Hartung, S. Hurling, K. Petermann and G. Huber, *Phys. Rev. B: Condens. Matter Mater. Phys.*, 1998, **57**, 2203–2216.
32 G. F. Li, D. G. Deng, Y. Q. Li, Q. Wang, Y. J. Hua and S. Q. Xu, *J. Rare Earths*, 2012, **30**, 193–196.
33 D. J. Newman, *Crystal Field Handbook*, Cambridge University Press, Cambridge, UK, 2000.
34 B. Z. Malkin, Crystal Field and Electron-Phonon Interaction in Rare-Earth Ionic Paramagnets, in *Spectroscopy of Solids Containing Rare-Earth Ions*, North Holland, Amsterdam, 1987.
35 B. C. Wang, Z. Y. Wang, Y. G. Liu, T. Yang, Z. H. Huang and M. H. Fang, *J. Alloys Compd.*, 2019, **776**, 554–559.

